

Backbone and shortest-path exponents of the two-dimensional Q -state Potts model

Sheng Fang,^{1,2} Da Ke,¹ Wei Zhong,^{1,*} and Youjin Deng^{1,2,3,†}

¹*MinJiang Collaborative Center for Theoretical Physics,*

College of Physics and Electronic Information Engineering, Minjiang University, Fuzhou 350108, China

²*Department of Modern Physics, University of Science and Technology of China, Hefei, Anhui 230026, China*

³*Shanghai Research Center for Quantum Sciences, Shanghai 201315, China*

(Dated: April 20, 2022)

We present a Monte Carlo study of the backbone and the shortest-path exponents of the two-dimensional Q -state Potts model in the Fortuin-Kasteleyn bond representation. We first use cluster algorithms to simulate the critical Potts model on the square lattice and obtain the backbone exponents $d_B = 1.7320(3)$ and $1.794(2)$ for $Q = 2, 3$, respectively. However, for large Q , the study suffers from serious critical slowing down and slowly converging finite-size corrections. To overcome these difficulties, we consider the $O(n)$ loop model on the honeycomb lattice in the densely packed phase, which is regarded to correspond to the critical Potts model with $Q = n^2$. With a highly efficient cluster algorithm, we determine from domains enclosed by the loops $d_B = 1.64339(5), 1.73227(8), 1.7938(3), 1.8384(5), 1.8753(6)$ for $Q = 1, 2, 3, 2 + \sqrt{3}, 4$, respectively, and $d_{\min} = 1.0945(2), 1.0675(3), 1.0475(3), 1.0322(4)$ for $Q = 2, 3, 2 + \sqrt{3}, 4$, respectively. Our estimates significantly improve over the existing results for both d_B and d_{\min} . Finally, by studying finite-size corrections in backbone-related quantities, we conjecture an exact formula as a function of n for the leading correction exponent.

I. INTRODUCTION

The Potts model [1, 2] is an extension of the celebrated Ising model and plays an important role in the theory of phase transition and critical phenomena. It also has broad applications in various fields like condensed-matter physics [2]. Given a connected graph $G \equiv (V, E)$ with V the vertex (site) set and E the edge set, each vertex has a spin of an integer value $\sigma = 0, 1, \dots, Q-1$, and two spins at the ends of an edge are coupled as $-J\delta_{\sigma_i, \sigma_j}$, where J represents the interaction strength and δ is the Kronecker delta function. Accordingly, the partition function can be written as

$$\mathcal{Z}_{\text{Potts}} = \sum_{\{\sigma\}} \prod_{\langle ij \rangle} e^{J\delta_{\sigma_i, \sigma_j}}, \quad (1)$$

where the inverse temperature β has already been set to be 1, the summation $\{\sigma\}$ is over all possible spin configurations, and $\langle ij \rangle$ is for all pairings of spins on the edges. For $Q = 2$, the Potts model reduces to the Ising model with the Ising coupling strength $K = J/2$.

The Potts model can be reformulated in graphical representations, including the Fortuin-Kasteleyn (FK) bond [3, 4] and Q -flow (loop) representations [5, 6]. Both the graphical representations can be obtained from the original spin representation by high-temperature expansion techniques, and, recently, these two graphical models also have been directly mapped onto each other with the introduction of a loop-cluster joint model [7].

The FK bond representation is also known as the random-cluster (RC) representation, in which each edge

is either empty or occupied. Each occupied bond has a statistical weight (relative to an empty one) as $v = \exp(J) - 1$, and each connected component (also called cluster) has a fugacity Q . The partition function of the RC model then reads as

$$\mathcal{Z}_{\text{RC}} = \sum_{A \subseteq G} v^{\mathcal{N}_b} Q^{\mathcal{N}_c}, \quad (2)$$

where the summation is over all possible subgraphs of G , and \mathcal{N}_b and \mathcal{N}_c represent the total numbers of occupied bonds and clusters, respectively. As an important consequence, the parameter Q can now take any nonnegative real number. For ferromagnetic coupling $J > 0$, the bond weight v is positive, and each configuration in Eq. (2) has a probability interpretation. As special cases, the RC model reduces to the standard bond percolation in the $Q \rightarrow 1$ limit, and the spanning tree or forest for $Q \rightarrow 0$ [4]. The FK representation has an important role in conformal field theory [8] and in stochastic Loewner evolution [9, 10], leading to much advanced theoretical progresses for the Potts model. Further, based on passing back and forth between the spin and FK representations, efficient cluster methods (i.e., the Swendsen-Wang (SW) [11] and Wolff algorithms [12]) are developed and widely used.

In addition to physical quantities from the original spin representation, the RC model has very rich geometric structures associated with FK random clusters, and a variety of critical exponents are used to characterize these geometric behaviors, which were first introduced in percolation [13–15]. The Euclidean diameter ξ_1 of the largest cluster acts as the correlation length and diverges as $\xi_1 \sim t^{-\nu}$, with $t \equiv (v_c - v)/v_c$ and v_c the critical point, and ν is frequently called the correlation-length exponent. The mass s of any critical cluster has a power-law dependence on its diameter ξ_s as $s \sim \xi_s^{d_F}$ for $s \gg 1$, with d_F the fractal dimension. In two dimensions (2D), the

* w.zhong@mju.edu.cn

† yjdeng@ustc.edu.cn

hull and the external perimeter of clusters can be further defined and have fractal dimensions d_{hull} and d_{EP} , respectively. For a pair of connected sites with distance $|\mathbf{x}| \gg 1$, the graph distance \mathcal{S} , i.e., the minimum length of all connecting paths between them, algebraically diverges as $\mathcal{S} \sim |\mathbf{x}|^{d_{\text{min}}}$, with d_{min} the shortest-path exponent. If a voltage difference is applied between these two sites, the total number N_{B} of bonds carrying nonzero current scales as $N_{\text{B}} \sim |\mathbf{x}|^{d_{\text{B}}}$, where d_{B} is called the backbone exponent. Further, the total number N_{red} of red bonds, which carry all the current, behaves as $N_{\text{red}} \sim |\mathbf{x}|^{d_{\text{red}}}$, with d_{red} the red-bond exponent.

In the past decades, the Q -state Potts model has been extensively studied [16–19]. In 2D, the Potts model exhibits a second-order phase transition for $Q \leq 4$, and the exact values of most critical exponents have been identified. In the Coulomb gas theory [18, 19], the Coulomb-gas coupling strength g relates to Q as

$$Q = 4 \cos^2(\pi g/4), \quad g \in [2, 4], \quad (3)$$

and the thermal and magnetic exponents of the leading and subleading renormalization fields are known as

$$\begin{aligned} y_{t1} &= 3 - 6/g, & y_{t2} &= 4 - 16/g, \\ y_{h1} &= \frac{(g+2)(g+6)}{8g}, & y_{h2} &= \frac{(g+10)(g-2)}{8g}, \end{aligned} \quad (4)$$

where the leading thermal exponent y_{t1} is the inverse of the correlation-length exponent ν as $y_{t1} = 1/\nu$. The subleading field, with $y_{t2} < 0$, governs the convergence of leading corrections; logarithmic corrections arise as Q approaches to 4, for which $y_{t2} \rightarrow 0$.

The fractal dimension d_{F} of FK clusters is identical to the leading magnetic exponent as $d_{\text{F}} = y_{h1}$, and the exact values of some other geometric exponents are [20]

$$\begin{aligned} d_{\text{hull}} &= 1 + 2/g, & d_{\text{EP}} &= 1 + g/8, \\ d_{\text{red}} &= (4 - g)(3g + 4)/g. \end{aligned} \quad (5)$$

However, there is still a set of geometric critical exponents, including d_{B} and d_{min} , whose exact values are unavailable. Monte Carlo simulations have been used to estimate them [21–26], and Table I lists some estimates of d_{B} and d_{min} .

In this work, we apply the SW and Wolff cluster methods to simulate the critical Potts model on the square lattice, expecting to obtain better results for d_{B} and d_{min} than those in Refs. [21–24, 26]. An improved algorithm is formulated to classify the occupied bonds into “bridges” and “nonbridges” [23]. From the fractal dimension of bridge-free clusters, we determine $d_{\text{B}} = 1.7320(3)$ for $Q = 2$ and $1.794(2)$ for $Q = 3$. The estimate of d_{B} for $Q = 2$ is consistent with Ref. [24], and for $Q = 3$ it nearly rules out the result in Ref. [21]. As Q increases, however, the cluster methods suffer from severe critical slowing-down and finite-size corrections become very strong, preventing us to obtain high precision of d_{B} for large Q .

(Q, g)	d_{B}	d_{min}
(1, 8/3)	1.643 36(10)[23]	1.130 77(2)[26]
present	1.643 39(5)	-
(2, 3)	1.732 1(4)[24]	1.094 0(2) [24]
present	1.732 27(8)	1.094 5(2)
(3, 10/3)	1.789 5(5)[27]	1.066 2(30) [22]
present	1.793 8(3)	1.067 5(3)
$(2+\sqrt{3}, 11/3)$	-	-
present	1.838 4(5)	1.047 5(3)
(4, 4)	1.873(4)[27]	-
present	1.875 3(6)	1.032 2(4)

TABLE I. Best estimates of d_{B} and d_{min} for the two-dimensional Potts model with $Q = 1, 2, 3, 2 + \sqrt{3}, 4$ and g is the Coulomb-gas coupling strength. These final quoted values and the error margins are estimated from a variety of fitting results by taking into account statistical and systematic errors.

We then consider the $O(n)$ loop model [28] on the honeycomb lattice, of which the configuration is a gas of non-intersecting loops. Let n be the fugacity of a loop and x be the statistical weight for a loop segment (an occupied bond); the partition function reads as

$$\mathcal{Z}_{\text{loop}} = \sum_{\text{loops}} x^{\mathcal{L}} n^{\mathcal{N}_{\ell}}, \quad (6)$$

where \mathcal{N}_{ℓ} is the number of loops and \mathcal{L} is the total length of all the loops. For $n = 1$, the loop model reduces to the flow (loop) representation of the honeycomb-lattice Ising model, with the coupling strength as $\tanh(K) = x$ [29].

The phase diagram of the $O(n)$ loop model is shown in Fig. 1. As the bond weight x is increased, the system undergoes a second-order phase transition x_+ from the dilute phase, consisting of small loops, into a critical densely-packed (DP) phase, where loops have fractal structures. The universality of the DP phase is governed by the line x_- of stable fixed points. The exact locations of $x_{\pm}(n)$ are known as [30]

$$1/x_{\pm} = \sqrt{2 \pm \sqrt{2 - n}}. \quad (7)$$

The two curves meet at $(n = 2, x_{\pm} = 1/\sqrt{2})$. In the language of universality, the $O(n)$ loop model on the critical branch x_+ (DP phase) corresponds to the tricritical (critical) Q -state Potts model with $Q = n^2$ [30, 31]. An interesting note is that, at x_+ , the $O(1)$ loop model is typically regarded as the critical Ising model instead of the tricritical one-state Potts model.

In other words, despite of the absence of an exact transformation between the loop model (6) and the Potts model (1), the two systems have the same Coulomb-gas coupling strength g as long as $Q = n^2$. This correspondence is expected to hold true for any real $0 \leq Q \leq 4$, where, for noninteger Q , the Potts model should be formulated in the FK bond representation. The relation between g and Q is still given by Eq. (3), with $g \in [2, 4]$ for x_- and $g \in [4, 6]$ for x_+ . Furthermore, Eqs. (4) and

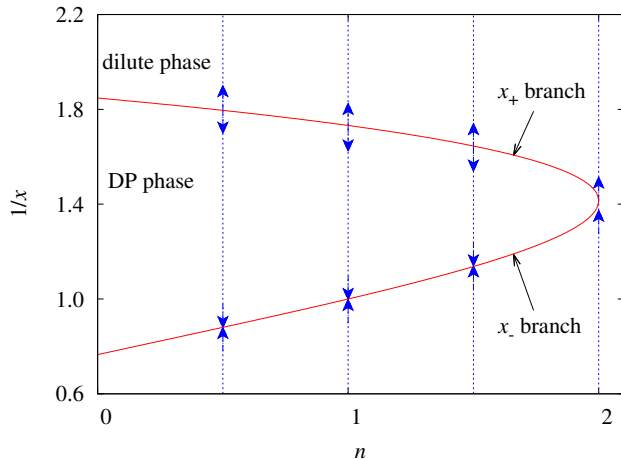


FIG. 1. Phase diagram of the $O(n)$ loop model on the honeycomb lattice. The system is in dilute phase if bond weight $x < x_+$ and in densely packed (DP) phase if $x > x_+$. Vertical blue arrows sketch the directions of renormalization flows, and illustrate that the whole DP phase ($x_+ < x < \infty$) is critical and in the same universality for each n .

(5) for critical exponents still hold true. However, what physical quantities in the loop model, described by these equations, need to be identified, and this has been largely explored in Refs. [32, 33]. The thermal field along the x direction has exponent y_{t2} in Eq. (4), instead of y_{t1} . The loops and the domains (faces) enclosed by the loops have the fractal dimensions d_{hull} and $d_F = y_{h1}$, respectively. The quantities, of which the scaling is governed by y_{t1} , are identified as the magnetization and the susceptibility of Ising spins living on the triangular lattice that is dual to the honeycomb lattice.

Highly efficient worm-type and cluster algorithms have been developed for the $O(n)$ loop model with $n \geq 1$ [32, 33]. It is shown that critical slowing-down barely exists at x_+ , and is completely absent in the DP phase, as qualitatively understood as following. For worm-type and cluster algorithms, the dynamic exponent z has the so-called Li-Sokal bound [34] $z \geq z_{\min} = \alpha/\nu$, where α/ν is the scaling exponent for specific heat, and, further, this lower bound is rather sharp $z \approx z_{\min}$ in 2D. For the critical Potts model, one has $z_{\min} = 2y_{t1} - 2$, leading to $z > 0$ for $Q > 2$. Moreover, as Q increases, the critical slowing-down becomes more severe, since y_{t1} is an increasing function of Q . However, the $O(n)$ loop model has $\alpha/\nu = 2y_{t2} - 2$, and thus, $z_{\min}(n \geq 1) \leq 0$ along x_+ and $z_{\min} < -2$ in the whole DP phase.

We aim to determine the backbone exponent d_B and the shortest-path exponent d_{\min} by studying the $O(n)$ loop model along the line $x_-(n)$. For this goal, we assume that the domains of DP loops and the corresponding FK random clusters not only have the same fractal dimension, but also exhibit the same scaling for other geometric properties. In comparison with the critical Potts model, the advantage of studying the loop model along

$x_-(n)$ is twofold: The absence of critical slowing-down and the absence of finite-size corrections from y_{t2} (corrections from other sources can still exist).

Our final estimates of d_B and d_{\min} are given in Table I, and significantly improve over the existing results. The agreement with the FK bond representation confirms our assumption that the domains of the DP $O(n)$ loops have the same geometric structures as the critical FK random clusters, and we expect that this correspondence can be extended to the x_+ branch.

In the analysis of quantities associated with bridge-free (backbone) clusters for the DP $O(n)$ loop model, we observe that, despite the absence of corrections from y_{t2} , finite-size corrections are still significant and become more and more severe as n increases. For the special case of $n = 2$, logarithmic corrections seem to arise. On the basis of our numerical results, we conjecture an exact formula, as a function of n , for the leading correction exponent.

The remainder of this paper is organized as follows. Algorithms for simulation and measurement are described in Sec. II, together with a list of sampled quantities. Section III presents our results for the backbone exponent and Sec. IV presents results for the shortest-path exponent. A brief discussion is given in Sec. V.

II. ALGORITHMS AND OBSERVABLES

A. Simulation of the Potts model

For integer Q , the celebrated SW and Wolff cluster algorithms are used, and, for real $Q \geq 1$, the Chayes-Machta (CM) method [35] is applied. They can be understood by the so-called *induced-subgraph* picture as following Ref. [32].

For the RC model (2) on graph $G = (V, E)$, one first decomposes Q as $Q = Q_\alpha + Q_\beta$. Independently for each cluster in a FK bond configuration, one then chooses color “ α ” with probability Q_α/Q or color “ β ” with probability Q_β/Q , and assigns the chosen color to all sites in the cluster. Consequently, the lattice sites are partitioned as $V = V_\alpha \cup V_\beta$, and the edge set E becomes $E = E_\alpha \cup E_\beta \cup E_{\alpha\beta}$; an edge $e \in E_{\alpha\beta}$ connects a pair of sites, respectively, in V_α and V_β , and it is not occupied by definition. It can be seen that, conditioning on this decomposition, the bond configuration is nothing other than the combination of a Q_α -state RC model on the induced subgraph $G_\alpha = (V_\alpha, E_\alpha)$ and another Q_β -state RC model on G_β . Now, one can update these induced RC models by any valid algorithm. One valid update is the identity operation, which is “do nothing” for the RC model, corresponding to the “inactive” color of Chayes and Machta [35]. Of course, we must also include at least one nontrivial update.

A simple choice is to set $Q_\alpha = 1$ for $Q \geq 1$, so that the corresponding induced model on G_α is the standard bond percolation and can be trivially updated, i.e., each edge

$e \in E_\alpha$ is independently occupied with probability p . On this basis, a basic variant of CM algorithm is formulated as:

1. Independently for each cluster, choose the active color “ α ” with probability $1/Q$ and otherwise “ β ” (inactive), resulting in a random partition $V = V_\alpha \cup V_\beta$ as well as $E = E_\alpha \cup E_\beta \cup E_{\alpha\beta}$.
2. Independently for each edge $e \in E_\alpha$, place an occupied bond with probability $p = v/(1+v)$ according to Eq. (2), and for $e \in E \setminus E_\alpha$, do nothing.

Here $E \setminus E_\alpha$ represents a complementary subset of E_α with edges in E_α being excluded. A new FK bond configuration is then obtained after ignoring/discarding the randomly assigned colors.

For $Q \geq 2$, the efficiency of the CM algorithm can be further improved by increasing the number of active colors to be $m = [Q]$, with $[Q]$ the ground integer of Q . Namely, for each cluster, an active color α_i ($i = 1, \dots, m$) is chosen with probability $1/Q$, leading to m copies of the bond percolation on G_{α_i} . For integer Q , where the “do-nothing” operation is absent, the celebrated SW algorithm is recovered. A single-cluster variant of the CM method is also available [36].

B. Simulation of the $O(n)$ model

The induced subgraph picture can also provide a versatile platform to design Monte Carlo algorithms for the $O(n)$ model (6) with $n \geq 1$. The basic idea is to set $n = n_\alpha + n_\beta$ with $n_\alpha = 1$, and to simulate the induced $O(1)$ loop model. More precisely, independently for each loop, one randomly assigns the active color “ α ” with probability $1/n$ and the inactive color “ β ” with probability $1 - 1/n$. In addition, one assigns the active color to all those sites that are not on loops, since they have an implicit weight of “1” (unity), as in Eq. (6). The $O(1)$ loop model on the induced subgraph can then be simulated by the worm algorithm. A variant of worm-type algorithm for the $O(n)$ loop model in 2D and 3D can be found in Refs. [33, 37].

Note that the honeycomb-lattice loops are the boundaries of Ising domains on the dual triangular lattice, with the one-to-two correspondence between the loop and the spin configuration of dual Ising spins. The dual coupling strength K^* relates to x as $2K^* = -\ln(x)$, which is ferromagnetic for $x < 1$ and antiferromagnetic for $x > 1$. The number of dual Ising domains is simply $\mathcal{N}_d = \mathcal{N}_\ell + 1$, with \mathcal{N}_ℓ the loop number and, thus, n is also the fugacity of an Ising domain. In other words, the $O(n)$ loop model can be regarded as a generalized Ising model on the triangular lattice, of which the partition function is written as

$$\mathcal{Z}_{\text{GIsn}} = \sum_{\{s\}} n^{\mathcal{N}_d} \prod_{\langle ij \rangle} \exp(K^* s_i s_j), \quad (8)$$

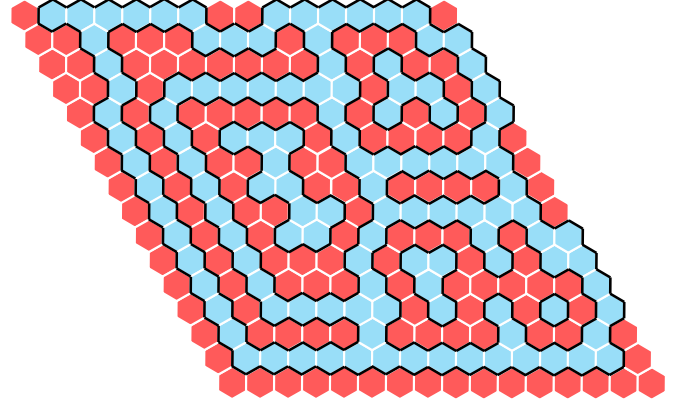


FIG. 2. Illustration of the generalized Ising model on the triangular lattice and the $O(n)$ loop model on the honeycomb lattice with periodic boundary conditions. The hexagons in red (blue) denote the spin-up (spin-down) sites and loops, i.e., the domain walls between the generalized Ising spins, are specified by blue lines.

where the summation is over all the Ising configurations. Figure 2 demonstrates the relation between the loop model and generalized Ising model. The Ising spins live on the sites of the triangular lattice, and the spin values are specified by the colors of the hexagonal faces. The domain walls are drawn between the boundaries of domains, which corresponds to the loops in the $O(n)$ loop model on the honeycomb lattice. In Fig. 2, there are $\mathcal{N}_d = 11$ domains and $\mathcal{N}_\ell = 10$ loops.

Applying the induced-subgraph picture to Eq. (8), one obtains a standard Ising model on induced subgraph G_α of the triangular lattice, which can be simulated by the SW or Wolff cluster algorithms. The bond-occupation probability is $p = 1 - e^{-2K^*} = 1 - x$ between a neighboring pair of parallel spins for $x \leq 1$ or $p = 1 - e^{2K^*} = 1 - 1/x$ between anti-parallel spins for $x > 1$. Nevertheless, some cautions are needed for the identify operation to the complementary subgraph $G \setminus G_\alpha$, which can no longer be “do-nothing”. Instead, one should place occupied bonds on all the edges $e \in E \setminus E_\alpha$, independent of the underlying Ising spins, so that all sites in V_β and their neighboring sites in V_α are in the same cluster. As a result, the domain topology on $G \setminus G_\alpha$ is kept unchanged, thanks to the Ising symmetry. For explicitness, the bond occupation probability for $x \leq 1$ is listed as

$$p = \begin{cases} 1 - x & \text{if } s_i = s_j \text{ and } i \in V_\alpha, j \in V_\alpha; \\ 0 & \text{if } s_i \neq s_j \text{ and } i \in V_\alpha, j \in V_\alpha; \\ 1 & \text{otherwise.} \end{cases} \quad (9)$$

For $x > 1$, similar procedure can be applied and the only difference is as follows: Within the active subgraph G_α , the bond is placed between antiparallel spins ($s_i \neq s_j$) with probability $p = 1 - 1/x$.

For the $O(n)$ loop model in the DP phase, both the cluster algorithm and the worm method exhibit no critical slowing-down, and their efficiency is approximately

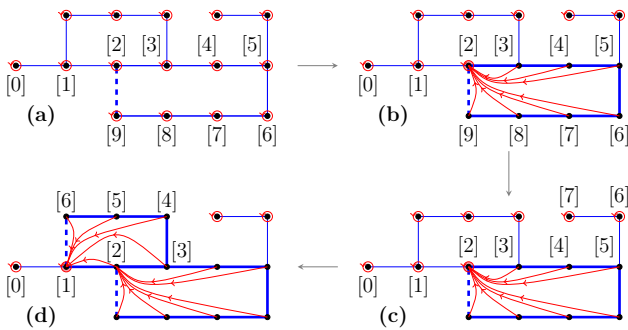


FIG. 3. Identification procedure for nonbridges. (a), Grow the depth-first oriented walk until it is a to-be-closed loop, as labeled by the walk $[0], [1], [2], \dots, [9]$. (b), Backtrack to the root site $[2]$, construct a flat tree (red arrows), and mark all the passing bonds as nonbridges (thick blue bonds). (c), Apply the last-in-first-out rule so that the old elements $[9], \dots, [6]$ are removed and new elements, $[6]$ and $[7]$, are added to the walk. (d), Add a new loop and replace the existing root by the new one. The final configuration consists of four bridge-free clusters, three of which are isolated sites (those with red circles).

the same. Since we are interested in the geometric structures of Ising domains in this work, simulating the generalized Ising model (8) can avoid the complication of passing back and forth between the honeycomb and the triangular lattice.

C. Identification of nonbridges

Following Ref. [23], we classify the occupied bonds of a FK bond configuration into bridges and nonbridges, and study the resulting bridge-free clusters to determine the backbone dimension d_B . A bridge is an occupied bond whose deletion would break a cluster into two, and removing all the bridges would produce a bridge-free configuration, which consists of isolated sites and blobs. In other terminology, blobs are also called bridge-free clusters and biconnected clusters, in which any two sites are connected by at least two independent paths. For the Ising domains on the triangular lattice, occupied bonds have to be first placed within the domains before the bond classification.

Two distinct methods to identify nonbridges are introduced in Refs. [23] and [38], of which the former makes use of the planarity of 2D lattices. In the latter, clusters are grown by breadth-first procedure with help of a tree-like data structure; whenever a newly visited bond is to close a loop, one backtracks the two branches of tree until the joint site, and all passing bonds are marked as nonbridges. A problem is that a nonbridge may be visited for many times. Since the number of nonbridges is of system size order, which is observed in Refs. [23, 24], a higher efficient algorithm is desired to identify nonbridges.

Hereby, we employ a depth-first growth with a chainlike data structure $\mathcal{W}[\ell]$ and introduce a treelike graph $\mathcal{D}[i]$ with some minimal depth. The chainlike array $\mathcal{W}[\ell]$ is to keep trace of the depth-first growth: Let $\mathcal{W}[\ell]$ denote the newly added site, $\mathcal{W}[\ell+1]$ stores the next to-be-added site. It is required that, at one step, only *one* of the unvisited sites connecting to $\mathcal{W}[\ell]$ is added, and thus the chain, $\mathcal{W}[0], \mathcal{W}[1], \dots, \mathcal{W}[\ell+1]$, is nothing other than an oriented walk. Further, the “last-in-first-out” rule is applied: If all neighboring sites of $\mathcal{W}[\ell]$ have been visited, then $\mathcal{W}[\ell]$ is removed and the incoming site $\mathcal{W}[\ell-1]$ becomes the walk frontier. Array $\mathcal{D}[i]$ is a directed graph consisting of many trees, and each tree is to represent a bridge-free cluster (including an isolated site). The parent site of site i is given by $\mathcal{D}[i]$, and the root of a tree is the site with the parent being itself. Initially, $\mathcal{D}[i] = i$ is set for all sites $i \in V$.

The procedure is sketched in Fig. 3. Starting with an initial site, the depth-first walk is performed until it is a to-be-closed loop, labeled by $[0], [1], \dots, [9]$ in Fig. 3(a). Then, the root is found starting from the joint site, $[2]$, and the loop is identified by backtracking $\mathcal{D}[i]$ (if applicable) or $\mathcal{W}[\ell]$ to the root. Meanwhile, all the passing bonds are marked as nonbridges (thick blue bonds) and all the passing sites take the root as their parent [Fig. 3(b)]. Afterwards, the depth-first walk is continued with the last-in-first-out rule, as illustrated by Fig. 3(c). When a new loop is added, the existing root is taken place by the new one if they are different [Fig. 3(d)]. In this way, it is kept that the parent $\mathcal{D}[i]$ of site i is always visited no later than site i itself, so that the loop identification by backtracking $\mathcal{D}[i]$ works properly. When all bonds in the cluster are visited, the depth-first walk is done, and all the nonbridges are successfully identified. As a by-product, all bridge-free clusters are constructed so that if one can further keep track of the sizes of trees, the associated quantities can be calculated immediately.

In the backtracking procedure for identifying a loop, $\mathcal{D}(i)$ has a higher priority than $\mathcal{W}[\ell]$: If $\mathcal{D}(i) \neq i$, then the backtracking is applied to $\mathcal{D}[i]$ instead of $\mathcal{W}[\ell-1]$. This is to avoid visiting a nonbridge for many times. In this work, we observe that trees $\mathcal{D}(i)$ are very flat and their typical depth is of a few units. In practice, the trees can be further flatten: When a loop is to be formed, one tries to continue the walk by visiting another neighboring site of $\mathcal{W}[\ell]$. In other words, a self-avoiding walk is performed as long as possible before the backtracking procedure. Therefore, the present method has a nearly optimal efficiency for identifying nonbridges.

Sampled quantities.—On the basis of bridge-free clusters, we sample the size of the largest cluster as $B_1 = \langle \mathcal{B}_1 \rangle$ and calculate the second moment of cluster sizes as $B_2 = L^{-2} \langle \sum \mathcal{B}^2 \rangle$, where the sum is over all bridge-free clusters \mathcal{B} and $\langle \cdot \rangle$ represents the ensemble average. For the $O(n)$ loop model, we also distinguish the spin-up domains from the spin-down ones, and calculate the averaged size $B_A = \langle (\mathcal{B}_{1\uparrow} + \mathcal{B}_{1\downarrow})/2 \rangle$.

To determine the shortest-path exponent d_{\min} , we use

the breadth-first algorithm to grow clusters; the number \mathcal{S} of layers after finishing the cluster growth corresponds to the maximum graph distance between the seed site and any other site in the cluster. We then sample the longest graph distance among all the clusters as $S_1 = \langle \mathcal{S}_1 \rangle$.

At criticality, these sampled quantities are expected to asymptotically diverge as a power-law scaling of linear system size L . More precisely, they behave as

$$\begin{aligned} S_1 &\sim L^{d_{\min}}, & \text{and} \\ B_1 \sim B_A \sim L^{d_B}, & & B_2 \sim L^{2d_B-d}. \end{aligned} \quad (10)$$

III. RESULTS FOR BACKBONE EXPONENT

We simulate the critical Q -state Potts model on the square lattice and the DP $O(n)$ loop model with system size L ranging from 4 to 8192. Periodic boundary conditions are implemented. For the Potts model, we take $Q = 2, 3$ and the exact critical point $v_c = \sqrt{Q}$. For the loop model, the simulation is at the branch $x_-(n)$ with $n = 1, \sqrt{2}, \sqrt{3}, \sqrt{2 + \sqrt{3}}, 2$, corresponding to $Q = 1, 2, 3, 2 + \sqrt{3}, 4$, respectively. We generate more than 10^8 independent samples for each system size $L < 256$, and no fewer than 10^7 independent samples for $L \geq 256$.

We perform least-squares fits to the finite-size scaling ansatz

$$\mathcal{O} = L^{y_{\mathcal{O}}} (a + b_1 L^{y_1} + b_2 L^{y_2}) + c_0, \quad (11)$$

where $\mathcal{O} = S_1, B_1, B_A, B_2$ and the corresponding exponent $y_{\mathcal{O}}$ is given by Eq. (10). The term with c_0 describes the background contribution of the system, and those with b_1 and b_2 account for leading and subleading finite-size corrections, respectively. In comparison with the leading scaling term with amplitude a , all the other three terms play a role of corrections. As a precaution against correction-to-scaling terms that we miss including in the fitting ansatz, we impose a lower cutoff $L \geq L_m$ on the data points admitted in the fits, and systematically study the effect on the residuals (denoted by χ^2) by increasing L_m . In general, the preferred fit for any given ansatz corresponds to the smallest L_m for which the goodness of the fit is reasonable and for which subsequent increases in L_m do not cause the χ^2 value to drop by vastly more than one unit per degree of freedom (DF). In practice, by “reasonable” we mean that $\chi^2/\text{DF} \approx 1$. The systematic error is obtained by comparing estimates from various reasonable fitting ansatz.

A. Estimate from the Potts model

The $Q \rightarrow 1$ Potts model is the standard bond percolation, and the geometric structures of critical percolation clusters on the square lattice have been extensively studied in Ref. [23], which gives $d_B = 1.643\,36(10)$.

Q	L_m	d_B	a	b_1	y_1	χ^2/DF
2	8	1.732 17(9)	0.7995(6)	0.1168(9)	-0.66(1)	4.0/7
	16	1.732 0(1)	0.8003(8)	0.121(4)	-0.68(2)	2.1/6
	32	1.732 0(2)	0.800(1)	0.12(1)	-0.68(5)	2.1/5
	16	1.732 23(8)	0.7990(5)	0.104(3)	-5/8	2.3/6
	32	1.732 1(1)	0.7995(8)	0.098(7)	-5/8	1.5/5
3	16	1.794 0(6)	0.638(7)	0.415(2)	-0.44(1)	10.0/6
	32	1.793 6(9)	0.64(1)	0.420(9)	-0.46(3)	9.8/5
	16	1.793 3(1)	0.647(1)	0.415(2)	-0.46	12.0/7
	32	1.793 5(2)	0.645(2)	0.421(4)	-0.46	9.8/6
	64	1.793 2(3)	0.648(3)	0.411(10)	-0.46	8.6/5

TABLE II. Fitting results of B_1 for the Ising model and of B_2 for the $Q = 3$ Potts model.

The Coulomb-gas coupling of the Ising model ($Q = 2$) is $g = 3$, and, according to Eq. (4), the subleading thermal and magnetic scaling fields have exponents $y_{t2} = -4/3$ and $y_{h2} = 13/24$, respectively. However, the subleading magnetic field with y_{h2} is considered to be redundant due the Z_2 symmetry of the Ising spins, and the subleading thermal field with y_{t2} is believed to play no role in the scaling of thermodynamic quantities in the spin representation. Indeed, finite-size corrections with

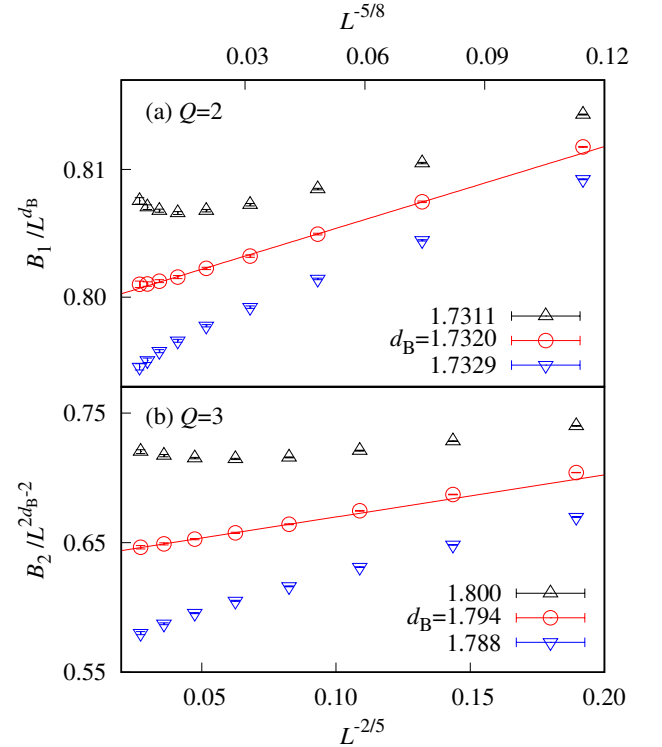


FIG. 4. Estimated backbone exponent d_B for the Ising model (a) and the $Q = 3$ Potts model (b). The approximate linearity of red lines indicates that the leading correction exponent is $y_1 \approx -0.6$ for $Q = 2$ and -0.4 for $Q = 3$. The upward and downward bending of other curves reflects the reliability of the finally quoted central values and their error bars.

exponent $y_{t2} = -4/3$ are not observed in physical observables; for quantities like energy, magnetization, specific heat, and susceptibility, the leading finite-size corrections are found to be governed by exponent -2 . Nevertheless, it remains open whether corrections with exponent $-4/3$ would arise in some geometric quantities.

According to the least-squares criterion, the B_1 data for $Q = 2$ are fitted to Eq. (11). At first, we set $b_2 = 0$ and leave d_B , a , b_1 , y_1 and c_0 as free parameters, but no stable fitting results can be obtained. By further fixing $c_0 = 0$, which is effectively a correction term, we obtain $d_B = 1.7320(2)$ and $y_1 = -0.68(5)$, of which the correction exponent is much larger than -2 or $-4/3$. The results are shown in Table II. Therefore, for geometric quantities associated with bridge-free clusters, the leading finite-size corrections probably arise from some other resource. In the framework of conformal field theory, an exponent $-5/8$ appears at several places in the Kac table for the Ising model [39]. With $y_1 = -5/8$ being fixed, the fit yields $d_B = 1.73223(8)$ for $L_m = 16$ (Table II). Following the same procedure, the fit of the B_2 data gives $d_B = 1.7323(5)$, which is consistent with d_B from B_1 but has a slightly larger error bar. Comparing the fitting results of B_1 and B_2 for different L_m , we take the final

estimate as $d_B = 1.7320(3)$. We choose not to seriously take into account the smaller error bar from the fits with $y_1 = -5/8$ being fixed, since it is only a crude guess and the exact value of y_1 is not available. In Fig. 4(a), the B_1/L^{d_B} data are plotted versus $L^{-5/8}$, with d_B chosen to be the central value of the estimate as well as the central value plus or minus three error bars. The approximate linearity of the red line and the upward and downward bending curves reflect the reliability of the final estimate $d_B = 1.7320$ and of the quoted error margin 0.0003 .

The leading correction exponent for the $Q = 3$ Potts model, with the Coulomb-gas coupling $g = 10/3$, is $y_{t2} = -4/5$. By fixing $b_2 = 0$ for the subleading correction term and $c_0 = 0$ for the background contribution, we fit the B_2 data to Eq. (11) and obtain $d_B = 1.7936(10)$ and $y_1 = -0.46(3)$. The value of y_1 is much larger than $y_{t2} = -4/5$, again suggesting that the leading finite-size corrections arise from some other source. The data are also well described when the term with c_0 is included and $y_1 = -0.46$ is fixed in Eq. (11), as shown in Table II. Corrections due to the subleading thermal field with $y_{t2} = -4/5$ should also exist, and, thus, there simultaneously exist corrections from different sources. Nevertheless, to identify different correction terms is very challenging for numerical analysis, particularly because our data are limited. The fits of B_1 yield $d_B = 1.792(2)$. To be conservative, we quote our final estimate as $d_B = 1.794(2)$, of which the reliability is demonstrated by Fig. 4(b).

We did not simulate the Potts model for larger value of Q , due to severe critical slowing-down and finite-size corrections.

B. Estimate from the loop model

For the $O(n)$ loop model, the backbone dimension d_B can be obtained from the finite-size scaling of quantities including B_1 , B_A , and S_2 , all of which give results consistent with each other. Nevertheless, the estimates from B_2 has somewhat better precision than those B_1 and B_A , probably because B_2 includes the sizes of all Ising domains in its definition. Table III summarizes the fitting results from B_2 for $n = 1, \sqrt{2}, \sqrt{3}, \sqrt{2} + \sqrt{3}$, corresponding to $Q = 1, 2, 3, 2 + \sqrt{3}$. The fitting details are given below.

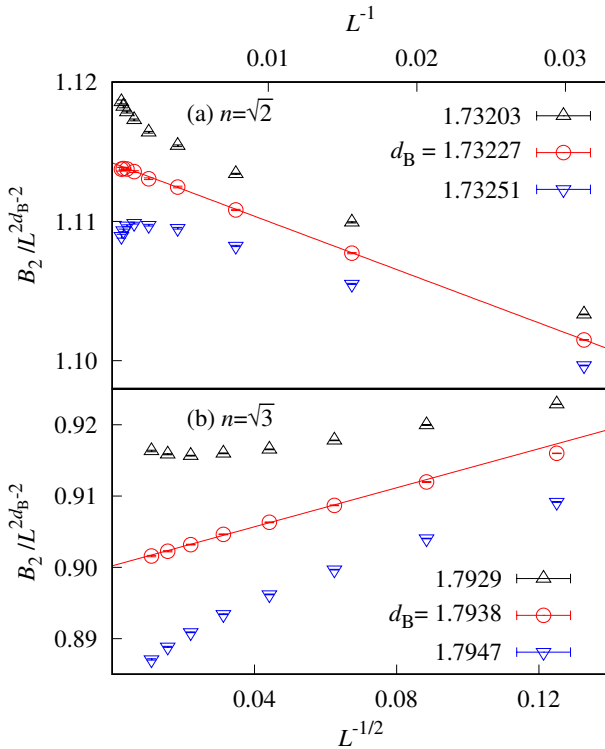


FIG. 5. Backbone exponent d_B for the DP $O(n)$ loop model with $n = \sqrt{2}$ (a) and $n = \sqrt{3}$ (b). The upward or downward bending of curves with the d_B value deviating from the estimated value illustrates the reliability of the quoted error bars. By comparing to Fig. 4, it is seen that the results from the loop model have higher precision.

From Eq. (7) for the line of stable fixed points, one has the bond weight $x = 1$ for $n = 1$, meaning that the coupling strength for the dual Ising model $K^* = -\frac{1}{2} \ln x = 0$ and thus the Ising spins on different lattice sites are independent. With up (down) spins being interpreted as occupied (empty) sites, the DP $O(1)$ loop model at the branch x_- is just the site percolation on the triangular lattice. This is also reflected in the induced-subgraph

cluster algorithm, as formulated in Sec. II, where the bond occupation probability $p = 1 - x = 0$ and each site is randomly occupied or empty with probability 50%.

In the least-squares fit of the second moment B_2 of bridge-free clusters by Eq. (11), if $b_2 = 0$ and b_1, y_1 and c_0 are left as free parameters, then we have $d_B = 1.64338(4)$ but the correction amplitude b_1 is consistent with zero within its error bar. With further fixing $c_0 = 0$, we obtain $d_B = 1.64339(2)$ and $y_1 = -1.09(1)$. The B_2 data can be also well described by Eq. (11) with $b_1 = b_2 = 0$ and c_0 as free parameter, and the backbone dimension is $d_B = 1.64335(5)$. The fitting results are listed in Table III. By considering all different fits, we take the final estimate as $d_B = 1.64339(5)$, of which the reliability is illustrated in Fig. 6. The fits for B_1 and B_A give $d_B = 1.64337(9)$ and $d_B = 1.64338(5)$, respectively, which are consistent with that from B_2 but have slightly larger error bars.

$$2. \quad n = \sqrt{2}$$

As described in Sec. II, the current study of the honeycomb-lattice $O(n)$ loop model is to simulate the generalized Ising model Eq. (8) on the triangular lattice by the induced-subgraph cluster method. To determine the backbone dimension d_B for $Q = 2$, one can either simulate the standard Ising model at the critical branch $1/x_+ = \sqrt{3}$ and study the FK random clusters constructed in the cluster simulation or simulate the $O(\sqrt{2})$ loop model in the DP phase and study the Ising domains. Namely, within the framework of the loop model, there exists a correspondence between the FK random clusters constructed at the critical branch x_+ with $n = 1$ and the Ising domains in the DP phase with $n^* = \sqrt{2}$.

We argue that such a geometric correspondence can be

Q	L_m	d_B	a	b_1	y_1	χ^2/DF
1	16	1.64339(1)	1.4922(2)	-1.529(9)	-1.082(3)	4.2/6
	32	1.64340(2)	1.4918(4)	-1.57(4)	-1.091(9)	3.0/5
	64	1.64339(2)	1.4921(6)	-1.5(1)	-1.08(2)	2.8/4
	32	1.64335(1)	1.4932(3)	-1.07(1)	-1	4.2/5
	64	1.64337(2)	1.4928(4)	-1.02(3)	-1	2.1/4
	32	1.73227(3)	1.1140(5)	-0.40(3)	-1.00(3)	5.4/4
2	64	1.73227(5)	1.1139(8)	-0.4(1)	-1.01(8)	5.3/3
	32	1.73227(1)	1.1140(2)	-0.399(3)	-1	5.4/5
	64	1.73227(2)	1.1140(3)	-0.400(8)	-1	5.4/4
	32	1.7939(1)	0.898(3)	0.105(4)	-0.42(3)	5.4/5
3	32	1.7938(2)	0.900(4)	0.11(1)	-0.46(6)	4.9/4
	32	1.79366(3)	0.9024(5)	0.126(3)	-1/2	5.4/5
	64	1.79370(5)	0.9018(8)	0.130(5)	-1/2	4.4/4
	32	1.8383(2)	0.757(3)	0.210(2)	-0.304(6)	4.5/6
+	16	1.8384(2)	0.755(5)	0.211(2)	-0.30(1)	4.3/5
	8	1.83838(3)	0.7546(4)	0.2114(7)	-0.3	5.0/7
	16	1.83836(4)	0.7549(5)	0.211(1)	-0.3	4.3/6
	32	1.83832(5)	0.7555(8)	0.209(2)	-0.3	3.5/5

TABLE III. Fitting results of d_B from B_2 for the DP $O(n)$ loop model with $n = 1, \sqrt{2}, \sqrt{3}, \sqrt{2} + \sqrt{3}$.

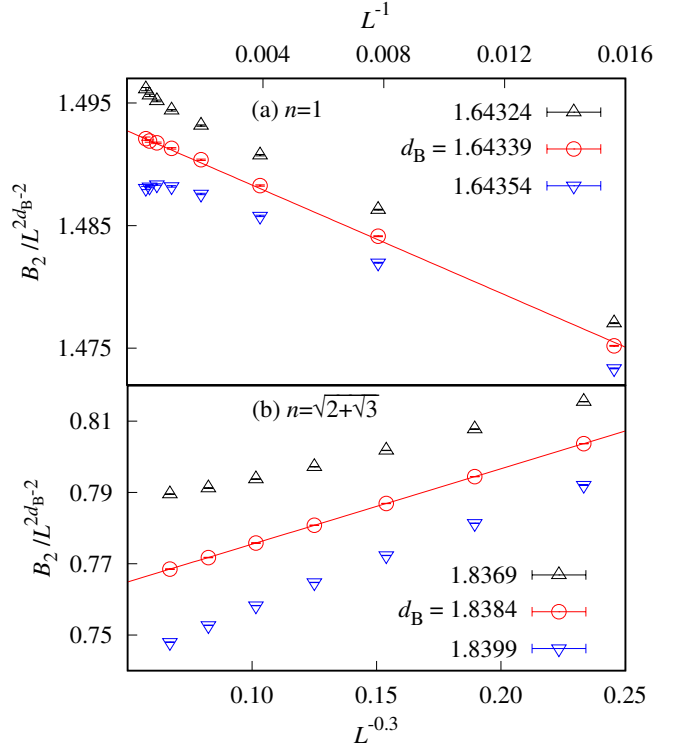


FIG. 6. Estimated backbone exponent d_B from the domains of the DP $O(n)$ loop model with $n = 1$ (a) and $n = \sqrt{2} + \sqrt{3}$ (b). The $O(1)$ loop model, which has the bond weight $x = 1$, is actually the site percolation on the triangular lattice. The upward or downward bending of those curves, with the d_B value deviating from the estimated value, illustrates the reliability of the quoted error bars.

extended to general n . Given the honeycomb-lattice loop model with parameters (n, x) , one can always construct on the triangular lattice the Ising domains and FK-like random clusters by placing occupied bonds with probability $1 - x$ within each domain. Along the critical branch $x_+(n)$, we assume the following duality relation: Both the fractal dimensions of domains and of FK-like random clusters, d_{FACE} and d_{FK} , are given by y_{h1} in Eq. (4); nevertheless, the Coulomb-gas coupling g for d_{FACE} is in [4, 6] and calculated from n as $n = -2 \cos(\pi g/4)$, while g_* for d_{FK} is in [2, 4] and relates to g as $g_* = 16/g$. As a consequence of this duality relation, we further argue that the FK-like random clusters for (n, x_+) have the same geometric structures as the domains of the DP $O(n_*)$ loop model with $n_* = -2 \cos(\pi g_*/4)$, similarly to the correspondence between the critical and tricritical Q -state Potts model observed in Ref. [27]. For the marginal case $n = n_* = 2$, this means that, apart from multiplicative logarithmic corrections, the FK-like random clusters and the domains have the same fractal dimension. Finally, it is noted that, for $n < 2$, the FK random clusters in the DP phase are too small to percolate. A simple example is for $(n = 1, x_- = 1)$, where the bond probability

is $p = 1 - x = 0$ and each FK-like cluster is just a single site.

For the critical Ising model, the induced-subgraph cluster method reduces to the SW cluster algorithm, which still suffers from some critical slowing-down due to the logarithmic divergence of the specific heat. Hereby, we determine the backbone dimension d_B from the $O(\sqrt{2})$ loop model at the branch x_- , for which critical slowing-down is completely absent.

We perform the least-squares fits for the B_2 data to Eq. (11). By setting $b_2 = 0$ and leaving the other correction parameters free, we obtain $d_B = 1.73219(5)$, and c_0 is consistent with zero within its error bar. By further fixing $c_0 = 0$, we have $d_B = 1.73227(5)$ and $y_1 = -1.01(8)$. The error bar of d_B can be further suppressed if $y_1 = -1$ is taken. Nevertheless, this smaller error bar cannot be taken into account seriously, since we are not aware from what sources such finite-size corrections arise. The fitting results are given in Table III, and the final estimate is quoted as $d_B = 1.73227(8)$, of which the reliability for the central value and the quoted error bar is illustrated in Fig. 5. The fits for B_1 and B_A give $d_B = 1.7322(1)$ and $d_B = 1.7320(3)$, respectively, in excellent agreement with that from B_2 .

3. $n = \sqrt{3}$

The same fitting procedure is applied to the data of B_1, B_A, B_2 . It is now necessary to simultaneously include two correction terms (e.g., with b_1 and c_0). For $n = \sqrt{3}$, we obtain $d_B = 1.7938(3)$ from B_2 , $1.7935(7)$ from B_1 and $1.7940(7)$ from B_A . The leading correction exponent is estimated as $y_1 = -0.42(3)$, which is in good agreement with $y_1 = -0.46(3)$ from the $Q = 3$ Potts model. Both estimates of y_1 are significantly larger than $y_{t2} = -2/5$. This strongly suggests that the leading corrections associated with backbone clusters are from some scaling field with exponent near ≈ -0.4 . The fitting results are listed in Table III, the final estimate is taken as $d_B = 1.7938(3)$ and shown Fig. 5(b).

4. $n = \sqrt{2 + \sqrt{3}}$

The Coulomb-gas coupling is $g = 11/3$, leading to $y_{t2} = -4/11 \approx -0.364$. With $b_2 = 0$, we obtain exponents $d_B = 1.8382(2)$ and $y_1 = -0.304(6)$ for $L_m = 8$, and the correction amplitudes are also well determined as $b_1 = 0.210(2)$ and $c_0 = -0.254(8)$. Although the estimated value of y_1 is larger than y_{t2} if the error bar of y_1 is taken into account, it is difficult to conclude $y_1 \neq y_{t2}$. Nevertheless, it is clear that, as n increases, finite-size corrections become larger and larger, albeit they are smaller than those for the corresponding Potts model. As $n \rightarrow 2$, we expect that correction exponent $y_1 \rightarrow 0$ and multiplicative logarithmic corrections would

L_m	y_{D_2}	a	b_1	y_1	χ^2/DF
4	1.750000(8)	0.89188(4)	0.079(4)	-2.00(4)	4.0/8
8	1.749993(10)	0.89192(5)	0.12(5)	-2.2(2)	2.7/7
4	1.750000(6)	0.89188(3)	0.0787(6)	-2	4.0/9
8	1.750001(7)	0.89187(3)	0.079(2)	-2	4.0/8

TABLE IV. Fitting results of the second moment D_2 of domain sizes for the $O(2)$ loop model at $x_{\pm} = 1/\sqrt{2}$.

arise. The final estimate is taken as $d_B = 1.8384(5)$ and shown in Fig. 6(b).

C. Logarithmic corrections for $n = 2$

The two branches of the $O(n)$ loop model meet at $x_{\pm} = 1/\sqrt{2}$ for $n = 2$, and the thermal field associated with the bond weight x becomes marginal (i.e., $y_{t2} = 0$). In accordance with the phase diagram in Fig. 1, this thermal field is marginally irrelevant for $x > x_{\pm}$ and marginally relevant for $x < x_{\pm}$, and, at x_{\pm} , its amplitude vanishes. It is expected that logarithmic corrections, irrespective of multiplicative or additive forms, are absent in thermodynamic quantities, including energy density, specific heat, and magnetic susceptibility, as well as in geometric quantities associated with the sizes of loops or domains.

To confirm this expectation, we sample the second moment of domain sizes as $D_2 = L^{-2} \langle \sum \mathcal{D}^2 \rangle$, where the summation is over all the dual Ising domains \mathcal{D} . The domains have a fractal dimension $d_F = y_{h1}$ given by Eq. (4),

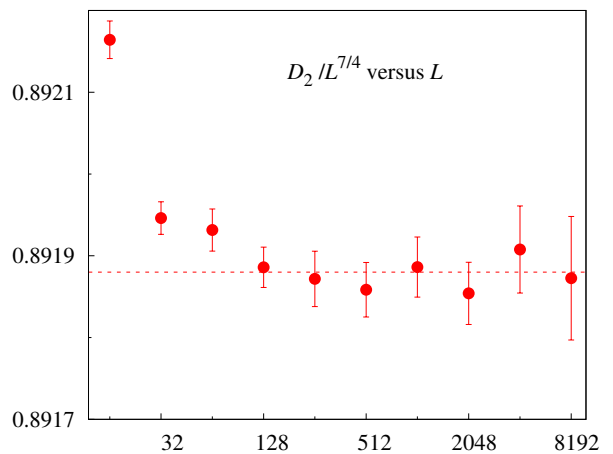


FIG. 7. Absence of multiplicative and additive logarithmic corrections in geometric quantities associated with domain sizes of the $O(2)$ loop model at $x_{\pm} = 1/\sqrt{2}$, as illustrated by the rescaled quantity $D_2/L^{7/4}$. The horizontal axis is the log plot of linear size L . All the finite-size data of $D_2/L^{7/4}$ are more or less consistent with the horizontal red dashed line at 0.89188, strongly indicating that corrections of logarithmic types are absent and those of algebraic forms are very small.

\mathcal{O}	L_m	d_B	a	b_1	y_1	χ^2/DF
B_2	16	1.867 1(3)	0.733(6)	0.230(3)	-0.29(1)	3.7/5
	32	1.866 7(4)	0.740(9)	0.230(2)	-0.30(2)	2.8/4
	64	1.866 9(8)	0.74(2)	0.229(3)	-0.29(4)	2.8/3
B_A	32	1.869(1)	0.522(9)	0.051(8)	-0.20(4)	1.5/4
	64	1.868(1)	0.531(10)	0.046(5)	-0.25(8)	0.9/3
B_1	16	1.866 4(6)	0.780(6)	0.149(3)	-0.30(2)	3.7/5
	32	1.866 2(9)	0.782(10)	0.149(2)	-0.31(4)	3.6/4

TABLE V. Fitting results for backbone exponent d_B for the O(2) loop model without logarithmic corrections-i.e., Eq. (11).

and, for $n = 2$, it is expected $D_2 \sim L^{2d_f-2} = L^{7/4}$ with $d_f = 15/8$. By fixing $b_2 = c_0 = 0$ so that only one single correction term is included in Eq. (11), we observe that the reasonably good fits can already be obtained with the minimum size as small as $L_m = 4$. The estimated exponent, $d_f = 1.875\,00(1)$, is in excellent agreement with the exact value $15/8$. The correction exponent $y_1 = -2.00(4)$ is well consistent with -2 , and, furthermore, the correction amplitude $b_1 = 0.079(4)$ is very small; see Table IV for details. For clarity, the rescaled data of $D_2/L^{7/4}$ are plotted versus size L in Fig. 7, and it can be seen that, as long as for $L \geq 128$, finite-size corrections are buried in statistical noise. The rapid convergence of $D_2/L^{7/4}$ demonstrates the absence of multiplicative or additive logarithmic corrections for $n = 2$. It also strongly supports that, along the line $x_-(n)$ of stable fixed points, finite-size corrections with y_{t2} should not occur in quantities associated with loops and domains.

For the backbone exponent d_B , we first try to fit the data to Eq. (11), without logarithmic corrections being included, and the results are shown Table V. Taking B_2 for an example, if we fix $b_2 = 0$ and leave other parameters free, then no stable results can be obtained. When $c_0 = 0$ is further fixed, we have $d_B = 1.866\,9(8)$. Similar analysis for B_A and B_1 gives $d_B = 1.868(2)$ and $1.866(2)$, respectively. As shown in Table V, all the estimates are consistent with each other. The estimated value of d_B is slightly smaller than the fractal dimension $d_f = 15/8$.

In the earlier study [21], it was numerically observed that the backbone exponent d_B of the tricritical Potts model reduces to the fractal dimension d_f of FK random clusters, which can be explained by the fact that the red-bond scaling field is irrelevant (i.e., $d_{\text{red}} < 0$ for $g > 4$). For the O(2) loop model with $g = 4$, the red-bond scaling field is marginal $d_{\text{red}} = 0$, and thus, $d_B = d_f = 15/8$ might still be expected. Nevertheless, the fitting results of d_B in Table V deviate from the predicted value systematically when the error bars are taken into account. A plausible reason is due to logarithmic corrections, which may still occur in backbone clusters. This is also implicitly reflected by the small correction exponent $y_1 \approx -0.2$, as shown in Table V, which might actually correspond to logarithmic corrections.

We assume that quantities on the basis of backbone

\mathcal{O}	L_m	d_B	a	b	$\hat{y}_\mathcal{O}$	d_0	χ^2/DF
B_2	64	1.875	1.171(3)	0.06(3)	-0.246(2)	1.928(4)	2.3/3
	128	1.875	1.171(8)	0.07(9)	-0.246(4)	1.929(9)	0.5/2
	128	1.875 6(3)	1.163(2)	-0.12(8)	-0.25	1.66(2)	2.1/2
B_A	16	1.875	0.694(4)	-0.042(2)	-0.126(2)	4.2(1)	5.1/6
	32	1.875	0.700(7)	-0.038(5)	-0.129(3)	4.4(3)	4.3/5
	16	1.874 93(8)	0.6919(9)	-0.042(2)	-0.125	4.13(7)	5.0/6
B_1	32	1.874 8(1)	0.693(2)	-0.039(4)	-0.125	4.2(1)	4.2/5
	16	1.875	0.960(6)	-0.01(1)	-0.120(2)	0.7(1)	4.3/6
	32	1.875	0.956(10)	-0.03(3)	-0.118(3)	0.6(2)	4.0/5
B_1	64	1.875	0.96(2)	-0.01(6)	-0.120(6)	0.7(4)	3.9/4
	16	1.875 3(1)	0.971(2)	-0.006(8)	-0.125	0.88(6)	4.3/6
	32	1.875 4(2)	0.970(3)	-0.01(2)	-0.125	0.8(1)	4.1/5
B_1	64	1.875 3(3)	0.972(5)	0.01(4)	-0.125	0.9(2)	3.9/4

TABLE VI. Fitting results of d_B for the O(2) loop model with the logarithmic ansatz (12) and $y_1 = -1$.

clusters follow the following finite-size scaling ansatz

$$\mathcal{O} = L^{y_\mathcal{O}} [\ln L + d_0]^{\hat{y}_\mathcal{O}} (a + bL^{y_1}), \quad (12)$$

where the constant d_0 is commonly used in the fitting with multiplicative logarithmic corrections. In comparison with the general scaling ansatz for logarithmic corrections, we have ignored in Eq. (12) additive logarithmic corrections which appear in powers of $1/\ln L$. This is because, in the fit, (i) the effects of parameter d_0 and of those additive logarithmic corrections can interfere with each other, and (ii) our data are limited and can already be reasonably described without multiplicative logarithmic corrections.

Since no prediction exists for the logarithmic exponent $\hat{y}_\mathcal{O}$ for backbone clusters and it is difficult to get an estimate to $y_\mathcal{O}$ and $\hat{y}_\mathcal{O}$ simultaneously, we first fix $y_\mathcal{O}$ with expected value and get the estimate of $\hat{y}_\mathcal{O}$. For B_2 , we first fix $y_\mathcal{O} = 2d_B - 2 = 7/4$ and leave all other parameters free, which leads to no stable results. Then we fix $y_1 = -1$ and obtain $\hat{y}_\mathcal{O} = -0.246(2)$ for $L_m = 64$. More fits have been done with y_1 fixed to various values in the interval $[-2, -1]$, which give the estimate $\hat{y}_\mathcal{O} = 0.24(1)$. Later, we fix $y_1 = -1$ and $\hat{y}_\mathcal{O}$ to various values in the range $-0.23 \leq \hat{y}_\mathcal{O} \leq -0.25$, and we obtain the estimate $d_B = 1.875\,3(6)$ by covering all the fitting results. Following the same procedure, we obtain the estimate $d_B = 1.874\,7(7)$ and $\hat{y}_\mathcal{O} = 0.135(15)$ for B_A , $d_B = 1.875\,2(7)$ and $\hat{y}_\mathcal{O} = 0.122(8)$ for B_1 . The detail of the fitting results are summarized in Table. VI. Thus, we expect $(y_\mathcal{O}, \hat{y}_\mathcal{O})$ is $(15/8, 1/8)$ for B_A and B_1 , and is $(7/4, 1/4)$ for B_2 . This is further demonstrated in Fig. 8, where the approximately straight lines in the log-log plot correspond to logarithmic exponents $\hat{y}_\mathcal{O} = -1/4$ and $-1/8$.

In the four-state Potts model, the multiplicative logarithmic correction exponent is $-1/16$ for the magnetization [40], and thus, the size of the largest FK cluster also has logarithmic exponent $-1/16$, half of our estimate $-1/8$ for backbone clusters. This is an interesting observation, but it might be due to the absence of additive

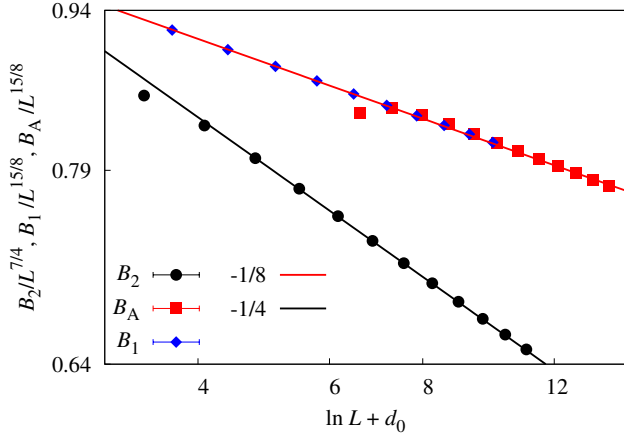


FIG. 8. Log-log plot of rescaled backbone quantities versus $(\ln L + d_0)$ for the $O(2)$ loop model. The rescaled quantities are $B_2/L^{7/4}$, $B_1/L^{15/8}$, and $B_A/L^{15/8}$. For being concise, B_A is multiplied by a constant such that the data for B_A and B_1 approximately collapse on top of each other. The existence of multiplicative logarithmic corrections and the corresponding exponents are clearly illustrated.

logarithmic corrections in Eq. (12). Unfortunately, it is very challenging to obtain conclusive evidence from fits simultaneously with multiplicative and additive logarithmic corrections. Further theoretical insights are needed for the exact value of the logarithmic exponent for backbone clusters at $n = 2$.

D. Conjectured formula for leading correction exponent in backbone clusters

The fitting results of d_B from the Q -state Potts and the DP $O(n)$ loop model suggest that, in geometric observables associated with backbone clusters, the leading correction exponent is $y_1 \approx -1.0, -0.6, -0.4, -0.2$ for $Q = 1, 2, 3, 2 + \sqrt{3}$, respectively [the estimate $y_1 \approx -1$ for the $O(\sqrt{2})$ loop model might be due to the small amplitude of the correction term]. For $Q = 4$ or $n = 2$, there exists a marginal scaling field, leading to multiplicative and additive logarithmic corrections. These corrections cannot be accounted by the scaling field with y_{t2} . It is tempting to identify the exact value of y_1 from the Kac table in the conformal field theory [41].

The Kac table is characterized by a pair of integers $i, j \geq 0$. The value of a scaling dimension $X_{i,j}$, which relates to the corresponding exponent y as $y = 2 - X$, is expressed as [39, 42]

$$X_{i,j} = \frac{[i(m+1) - jm]^2 - 1}{2m(m+1)}, \quad (13)$$

where the conformal anomaly m can be calculated from the Coulomb-gas coupling as $m = g/(4 - g)$ for $g \in [2, 4]$ and $m = 4/(g - 4)$ for $g \in [4, 6]$. For the critical Potts

Q	L_m	d_B	a	b_1	b_2	χ^2/DF
1	64	1.643 34(2)	1.4935(5)	-0.67(3)	-5.8(8)	2.0/4
	128	1.643 33(3)	1.4937(8)	-0.69(7)	-5(4)	2.0/3
2	16	1.732 20(2)	1.1153(3)	-0.051(3)	-0.57(1)	8.3/6
	32	1.732 17(3)	1.1159(6)	-0.059(6)	-0.53(3)	6.3/5
	64	1.732 20(5)	1.1154(9)	-0.05(1)	-0.6(1)	5.6/4
3	64	1.794 1(1)	0.894(2)	0.108(9)	-0.04(2)	6.8/4
	128	1.793 8(2)	0.899(3)	0.07(2)	0.06(6)	3.2/3
	256	1.794 0(3)	0.895(6)	0.10(4)	-0.0(1)	2.5/2
2	32	1.840 0(3)	0.714(5)	0.14(1)	0.102(7)	1.6/5
+	64	1.840 0(4)	0.715(9)	0.14(2)	0.10(1)	1.6/4
$\sqrt{3}$	128	1.839 3(7)	0.73(2)	0.10(4)	0.13(3)	0.3/3

TABLE VII. Fitting results of d_B from B_2 for the DP $O(n)$ loop model with $n = 1, \sqrt{2}, \sqrt{3}, \sqrt{2 + \sqrt{3}}$. The leading correction exponent y_1 is fixed at the value given by Eq. (14) and the subleading correction exponent is taken as $y_2 = 2y_1$.

model, this gives $m = 2, 3, 5, \infty$ for $Q = 1, 2, 3, 4$, respectively. The exactly known exponents, in Eqs. (4) and (5) can be mostly identified in the Kac table with integer (i, j) . An exception is the leading magnetic dimension X_{h1} , of which the indices $i = j = (m+1)/2$ are half integers for $m = 2$ (percolation).

On the basis of the estimated values of y_1 , we conjecture that the corresponding indices are $(i, j) = (2, 0)$, leading to

$$y_1 = -(4m+3)/2m(m+1), \\ = -(4-g)(g+12)/8g. \quad (14)$$

This predicts $y_1 = -11/12, -5/8, -23/60, -47/263$ for $Q = 1, 2, 3, 2 + \sqrt{3}$, respectively, which are surprisingly close to the numerical results of y_1 . Moreover, Eq. (14) gives $y_1 \rightarrow 0$ as $g \rightarrow 4$, and thus can explain the appearance of logarithmic corrections for $n = 2$.

For the critical Q -state Potts model, the external-perimeter fractal dimension d_{ep} has indices as $(i, j) = (1, 0)$ in the Kac table, which is neighboring to $(i, j) = (2, 0)$ conjectured for y_1 . It is noted that d_{ep} is also the fractal dimension of external perimeters and hulls of backbone clusters [43]. This observation indirectly supports that the conjectured formula (14) might be reasonable for backbone clusters.

On this basis, we reanalyze the B_2 data for the DP $O(n)$ loop model by Eq. (11) with y_1 being fixed at the predicted value. Another correction term with b_2 or c_0 is also included, and, for simplicity, we first fix the subleading correction exponent as $y_2 = -2$. For $n = 1$, the fit with $c_0 = 0$ gives $d_B = 1.643 33(3)$, and the fit with $b_2 = 0$ leads to $d_B = 1.643 35(5)$, consistent with each other. The same procedure has been done for $n = \sqrt{2}$ and $\sqrt{3}$, and the results are consistent with the previous estimates. For $n = \sqrt{2 + \sqrt{3}}$, the residual χ^2 is big until $L_m = 128$, and the result is $d_B = 1.841 7(5)$ for $c_0 = 0$. When fixing $b_2 = 0$ and leaving c_0 free, we obtain $d_B = 1.841 5(5)$. Both estimates deviate from the previous estimate 1.838 5(4). This is probably due to that

Q	L_m	d_{\min}	a	b_1	y_1	χ^2/DF
2	32	1.094 42(7)	1.1221(6)	-2.01(3)	-0.943(5)	2.3/4
	64	1.094 5(1)	1.1212(9)	-2.10(8)	-0.96(1)	1.1/3
	64	1.094 54(3)	1.1209(3)	-2.132(7)	-0.96	1.2/4
	128	1.094 53(5)	1.1210(4)	-2.14(2)	-0.96	1.1/3
3	32	1.067 45(9)	1.0833(8)	-1.82(3)	-0.911(6)	2.7/4
	64	1.067 5(1)	1.082(1)	-1.9(1)	-0.92(2)	2.1/3
	32	1.067 58(3)	1.0822(2)	-1.865(3)	-0.92	5.0/5
	64	1.067 52(5)	1.0826(4)	-1.878(9)	-0.92	2.1/4
+ $\sqrt{3}$	128	1.067 52(7)	1.0826(6)	-1.88(2)	-0.92	2.1/3
	32	1.047 4(1)	1.0332(9)	-1.71(3)	-0.907(8)	4.2/4
	64	1.047 5(2)	1.033(2)	-1.7(1)	-0.91(2)	4.1/3
	32	1.047 49(4)	1.0328(3)	-1.724(4)	-0.91	4.4/5
4	64	1.047 47(6)	1.0330(4)	-1.73(1)	-0.91	4.1/4
	128	1.047 49(9)	1.0328(7)	-1.72(2)	-0.91	4.0/3
	32	1.031 9(1)	0.981(1)	-1.46(3)	-0.874(9)	4.1/4
	64	1.032 1(2)	0.980(2)	-1.6(1)	-0.90(2)	2.6/3
	64	1.032 15(7)	0.9795(5)	-1.59(1)	-0.9	2.6/4
	128	1.032 2(1)	0.9794(7)	-1.58(2)	-0.9	2.6/3

TABLE VIII. Fitting results of the shortest-path exponent d_{\min} from S_1 for the DP $O(n)$ loop model with $n = \sqrt{2}, \sqrt{3}, \sqrt{2 + \sqrt{3}}, 2$.

subleading finite-size corrections cannot be described by exponent $y_2 = -2$.

We then set $y_2 = 2y_1$ and fix $c_0 = 0$. The final estimates $d_B = 1.643\,33(3), 1.732\,20(6), 1.793\,9(4), 1.839\,5(9)$ are obtained for $n = 1, \sqrt{2}, \sqrt{3}$, and $\sqrt{2 + \sqrt{3}}$, respectively, consistent with previous estimates. The fitting results with this choice are summarized in Table VII. For $n = \sqrt{2}$, we have $y_2 = 2y_1 = -5/4$, close to -1 . The amplitude b_1 is much smaller than b_2 , and thus, for small system sizes, the subleading corrections can surpass the leading ones. This might explain that, in the previous fits, the estimated correction exponent is $y_1 \approx -1$ in Table III. For small n , the precision of d_B with this choice is slightly improved.

IV. RESULTS FOR SHORTEST-PATH EXPONENT

Since the shortest-path exponent d_{\min} of percolation ($Q \rightarrow 1$) is already estimated to have a high precision [26], we hereby present the results from the domains of the DP $O(n)$ loop model with $n = \sqrt{2}, \sqrt{3}, \sqrt{2 + \sqrt{3}}$, and 2. We perform the least-squares fits to the S_1 data by the ansatz (11). For $n = \sqrt{2}$, we first leave all parameters free but cannot get stable results. Then, we fix $c_0 = b_2 = 0$ and obtain the estimate $d_{\min} = 1.094\,48(13)$ and $y_1 \approx -0.96$, close to -1 . If we fix $y_2 = -2$ and leave b_2 free, then the fit gives the consistent estimate as $d_{\min} = 1.094\,5(1)$ and $y_1 = -0.97(2)$. In addition, fixing $y_1 = -1$ and leaving c_0 free gives the estimate $d_{\min} = 1.094\,5(1)$. We take the final estimate $d_{\min} = 1.094\,5(2)$ by considering the systematic error from different fits. Following the same procedure for $n = \sqrt{3}, \sqrt{2 + \sqrt{3}}, 2$,

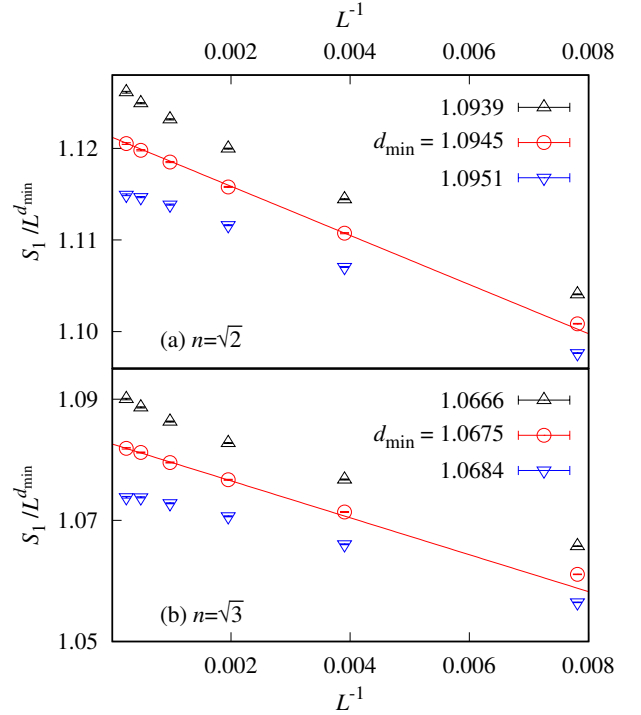


FIG. 9. Estimated shortest-path exponent d_{\min} from the domains of the DP $O(n)$ loop model with $n = \sqrt{2}$ (a) and $n = \sqrt{3}$ (b). The upward or downward bending of those curves, with the d_{\min} value deviating from the estimated value, illustrates the reliability of the quoted error bars.

we obtain $d_{\min} = 1.067\,5(3), 1.047\,5(3), 1.032\,2(4)$, respectively. The details of fits are summarized in Table VIII.

As shown in Table VIII, we find that the leading correction exponents y_1 is always close to -1 , irrespective of the value of n , and, thus, that the precision of d_{\min} remains approximately unchanged as n increases. Unlike for the backbone exponent d_B , finite-size corrections do not become stronger as n increases. In particular, no logarithmic corrections seem to arise for $n = 2$. In Figs. 9 and 10, we plot $S_1/L^{d_{\min}}$ versus L^{-1} . The approximate linearity of the red line and the upward and downward bending curves reflect the reliability of the estimates and the quoted error bars.

V. DISCUSSION

By cluster Monte Carlo methods, we carry out extensive simulations of the Q -state Potts model on the square lattice and of the $O(n)$ loop model on the honeycomb lattice, up to linear size $L = 8192$. The induced-subgraph picture adds a valuable perspective to understand the celebrated Swendsen-Wang algorithm and further provides a versatile platform to formulate efficient cluster or worm-type algorithms for loop models.

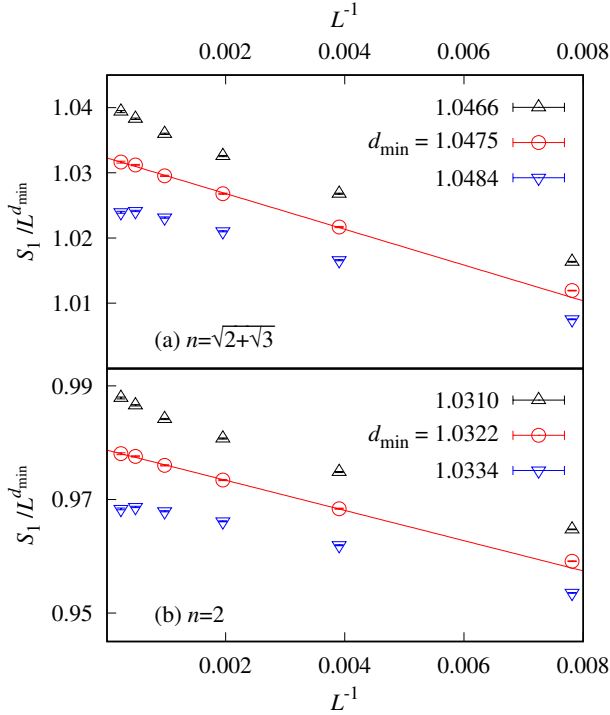


FIG. 10. Estimated shortest-path exponent d_{\min} from the domains of the DP $O(n)$ loop model with $n = \sqrt{2} + \sqrt{3}$ (a) and $n = 2$ (b). The upward or downward bending of those curves, with the d_{\min} value deviating from the estimated value, illustrates the reliability of the quoted error bars.

The backbone exponent d_B and the shortest-path exponent d_{\min} are determined for the Fortuin-Kasteleyn random clusters of the critical Potts model and for the domains of the DP $O(n)$ loop model. According to Coulomb gas theory, the DP $O(n)$ loop model corresponds to the critical Q -state Potts model with $Q = n^2$. The excellent agreement of the d_B and d_{\min} results between the two systems strongly supports that, in addition to the overall fractal structure, the domains of the DP loop model and the corresponding FK random clusters share the same scaling for other geometric properties.

In comparison with the Q -state Potts model, the study of the DP $O(n)$ loop model benefits from the advantages that the absence of critical slowing down and the absence of finite-size corrections with exponent y_{t2} in Eq. (4). Also, an improved algorithm for identifying backbones

is formulated, by adopting a depth-first cluster growth procedure and introducing an auxiliary array of treelike structure.

As a consequence of these advantages, the estimates of d_B and d_{\min} achieve a precision better than the existing results. It can be seen that, as Q increases, the backbone exponent d_B increases and the shortest-path exponent d_{\min} decreases, and, for $Q = 4$, the backbone exponent and the fractal dimension coincide (apart from logarithmic corrections). This reflects that the critical FK random clusters become more and more compact as Q increases. Since the exact values of d_B and d_{\min} are still unknown for the two-dimensional Potts model, our high-precision results can provide a solid testing ground for future theoretical explorations.

Finite-size corrections in the DP $O(n)$ loop model are also studied along the line of stable fixed points. It is confirmed that corrections with exponent y_{t2} are absent. Particularly, for the marginal case $n = 2$, multiplicative and additive logarithmic corrections are not observed in quantities associated with the domain sizes and in the shortest path. The leading correction exponent y_1 for the shortest path is observed to be roughly around -1 , independent of n . For backbone clusters, however, finite-size corrections become larger and larger as n increases, and logarithmic corrections arise for $n = 2$. To account for these corrections, which are beyond the description of exponent y_{t2} , we conjecture an exact formula, Eq. (14), for the correction exponent y_1 . The predicted value of y_1 is consistent with our Monte Carlo data, and can explain the emergence of logarithmic corrections for $n = 2$. Fixing the y_1 value can lead to smaller error bars of d_B , which are, however, not taken in our final estimate. It remains as an interesting question to explore whether our conjecture holds true.

VI. ACKNOWLEDGMENTS

Y.D. acknowledges support by the National Natural Science Foundation of China (under Grant No. 11625522), the Science and Technology Committee of Shanghai (under grant No. 20DZ2210100), and the National Key R&D Program of China (under Grant No. 2018YFA0306501). W.Z. acknowledges support by the National Natural Science Foundation of China Youth Fund (under Grant No. 12105133) and the Fujian Provincial Natural Science Foundation of China (under Grant No. 2021J011030).

-
- [1] R. B. Potts, Some generalized order-disorder transformations, in *Mathematical Proceedings of the Cambridge Philosophical Society*, Vol. 48 (Cambridge University Press, Cambridge, UK, 1952), pp. 106–109.
 [2] F. Y. Wu, The Potts model, *Reviews of Modern Physics* **54**, 235 (1982).

- [3] P.W. Kasteleyn and C.M. Fortuin, Phase transitions in lattice systems with random local properties, *Physical Society of Japan Journal Supplement* **26**, 11 (1969).
 [4] G. Grimmett, *The Random-Cluster Model*, edited by H. Kesten (Springer, Berlin, 2006).

- [5] J. W. Essam and C. Tsallis, The Potts model and flows I. The pair correlation function, *Journal of Physics A: Mathematical and General* **19**, 409 (1986).
- [6] F. Y. Wu, Potts model and graph theory, *Journal of Statistical Physics* **52**, 99 (1988).
- [7] L. Zhang, M. Michel, E. M. Elçi, and Y. Deng, Loop-cluster coupling and algorithm for classical statistical models, *Physical Review Letters* **125**, 200603 (2020).
- [8] P. Francesco, P. Mathieu, and D. Sénéchal, *Conformal Field Theory* (Springer Science & Business Media, New York, 2012).
- [9] W. Kager and B. Nienhuis, A guide to stochastic Löwner evolution and its applications, *Journal of Statistical Physics* **115**, 1149 (2004).
- [10] J. Cardy, SLE for theoretical physicists, *Annals of Physics* **318**, 81 (2005).
- [11] R. H. Swendsen and J. S. Wang, Nonuniversal critical dynamics in Monte Carlo simulations, *Physical Review Letters* **58**, 86 (1987).
- [12] U. Wolff, Collective Monte Carlo updating for spin systems, *Physical Review Letters* **62**, 361 (1989).
- [13] H. J. Herrmann and H. E. Stanley, Building blocks of percolation clusters: Volatile fractals, *Physical Review Letters* **53**, 1121 (1984).
- [14] H. J. Herrmann, D. Hong, and H. Stanley, Backbone and elastic backbone of percolation clusters obtained by the new method of ‘burning’, *Journal of Physics A: Mathematical and General* **17**, L261 (1984).
- [15] D. Stauffer and A. Aharony, *Introduction to Percolation Theory* (CRC Press, Boca Raton, FL, 2018).
- [16] R. J. Baxter, *Exactly solved models in statistical mechanics* (Elsevier, 2016).
- [17] F. Y. Wu, *Exactly Solved Models: A Journey In Statistical Mechanics-Selected Papers With Commentaries (1963–2008)* (World Scientific, 2009).
- [18] B. Nienhuis, Critical behavior of two-dimensional spin models and charge asymmetry in the Coulomb gas, *Journal of Statistical Physics* **34**, 731 (1984).
- [19] B. Nienhuis, Coulomb gas formulation of two-dimensional phase transitions, in *Phase transitions and Critical Phenomena*, Vol. 11, edited by C. Domb and J. L. Lebowitz (Academic Press, London, 1987) pp. 1–51.
- [20] A. Coniglio, Fractal structure of Ising and Potts clusters: Exact results, *Physical Review Letters* **62**, 3054 (1989).
- [21] Y. Deng, H. W. J. Blöte, and B. Nienhuis, Backbone exponents of the two-dimensional q -state Potts model: A Monte Carlo investigation, *Physical Review E* **69**, 026114 (2004).
- [22] Y. Deng, W. Zhang, T. M. Garoni, A. D. Sokal, and A. Sportiello, Some geometric critical exponents for percolation and the random-cluster model, *Physical Review E* **81**, 020102(R) (2010).
- [23] X. Xu, J. Wang, Z. Zhou, T. M. Garoni, and Y. Deng, Geometric structure of percolation clusters, *Physical Review E* **89**, 012120 (2014).
- [24] P. Hou, S. Fang, J. Wang, H. Hu, and Y. Deng, Geometric properties of the Fortuin-Kasteleyn representation of the Ising model, *Physical Review E* **99**, 042150 (2019).
- [25] E. M. Elçi, M. Weigel, and N. G. Fytas, Bridges in the random-cluster model, *Nuclear Physics B* **903**, 19 (2016).
- [26] Z. Zhou, J. Yang, Y. Deng, and R. M. Ziff, Shortest-path fractal dimension for percolation in two and three dimensions, *Physical Review E* **86**, 061101 (2012).
- [27] Y. Deng, H. W. J. Blöte, and B. Nienhuis, Geometric properties of two-dimensional critical and tricritical Potts models, *Physical Review E* **69**, 026123 (2004).
- [28] E. Domany, D. Mukamel, B. Nienhuis, and A. Schwimmer, Duality relations and equivalences for models with $O(n)$ and cubic symmetry, *Nuclear Physics B* **190**, 279 (1981).
- [29] C. J. Thompson, *Mathematical statistical mechanics* (Princeton University Press, 2015).
- [30] B. Nienhuis, Exact critical point and critical exponents of $O(n)$ models in two dimensions, *Physical Review Letters* **49**, 1062 (1982).
- [31] B. Nienhuis, Locus of the tricritical transition in a two-dimensional q -state Potts model, *Physica A: Statistical Mechanics and Its Applications* **177**, 109 (1991).
- [32] Y. Deng, T. M. Garoni, W. Guo, H. W. J. Blöte, and A. D. Sokal, Cluster simulations of loop models on two-dimensional lattices, *Physical Review Letters* **98**, 120601 (2007).
- [33] Q. Liu, Y. Deng, and T. M. Garoni, Worm Monte Carlo study of the honeycomb-lattice loop model, *Nuclear Physics B* **846**, 283 (2011).
- [34] X.-J. Li and A. D. Sokal, Rigorous lower bound on the dynamic critical exponents of the Swendsen-Wang algorithm, *Physical Review Letters* **63**, 827 (1989).
- [35] L. Chayes and J. Machta, Graphical representations and cluster algorithms II, *Physica A: Statistical Mechanics and Its Applications* **254**, 477 (1998).
- [36] Y. Deng, X. Qian, and H. W. J. Blöte, Single-cluster dynamics for the random-cluster model, *Physical Review E* **80**, 036707 (2009).
- [37] Q. Liu, Y. Deng, T. M. Garoni, and H. W. Blöte, The $O(n)$ loop model on a three-dimensional lattice, *Nuclear Physics B* **859**, 107 (2012).
- [38] W. Huang, P. Hou, J. Wang, R. M. Ziff, and Y. Deng, Critical percolation clusters in seven dimensions and on a complete graph, *Physical Review E* **97**, 022107 (2018).
- [39] J. Cardy, Conformal invariance, in *Phase transitions and Critical Phenomena*, Vol. 11, edited by C. Domb and J. L. Lebowitz (Academic Press, London, 1987) pp. 55–123.
- [40] J. Salas and A. D. Sokal, Logarithmic corrections and finite-size scaling in the two-dimensional 4-state Potts model, *Journal of Statistical Physics* **88**, 567 (1997).
- [41] M. Henkel, *Conformal invariance and critical phenomena* (Springer Science & Business Media, 1999).
- [42] D. Friedan, Z. Qiu, and S. Shenker, Conformal invariance, unitarity, and critical exponents in two dimensions, *Physical Review Letters* **52**, 1575 (1984).
- [43] T. Grossman and A. Aharony, Structure and perimeters of percolation clusters, *Journal of Physics A: Mathematical and General* **19**, L745 (1986).